

# Feedback of 10–20-day intraseasonal oscillations on seasonal mean SST in the tropical Western North Pacific during boreal spring through fall

Renguang Wu<sup>1,2</sup>

Received: 20 June 2016 / Accepted: 12 September 2016 / Published online: 19 September 2016  
© Springer-Verlag Berlin Heidelberg 2016

**Abstract** The present study documents the factors for year-to-year changes in the intensity of 10–20-day intraseasonal oscillations (ISOs) and investigates the feedback of the 10–20-day ISO intensity on seasonal mean sea surface temperature (SST) change in the tropical western North Pacific during boreal spring through fall. An analysis of local correlation reveals a significant negative correlation of the 10–20-day ISO intensity and the seasonal mean SST tendency in the tropical western North Pacific during spring, summer, and fall, suggesting a plausible feedback of the ISO intensity on seasonal mean SST anomaly. The 10–20-day ISO intensity change over the tropical western North Pacific is influenced by El Niño-Southern Oscillation (ENSO) through modulation of vertical shear of zonal winds, lower-level moisture, and upward motion. Due to the phase dependence of location of these ENSO-induced background field changes, the ISO intensity is subject to

ENSO influence in different regions during the three seasons. The feedback of the 10–20-day ISO intensity on local seasonal mean SST change in the tropical western North Pacific is demonstrated by separating latent heat flux anomalies into components on different time scales. The ISO-induced latent heat flux anomalies may accumulate in a season and overcome interannual anomalies due to seasonal mean changes. Thus, the ISO-induced surface heat flux change may play an important role in the seasonal mean SST anomaly in the tropical western North Pacific.

**Keywords** ISO feedback · Seasonal mean SST · Latent heat flux decomposition · Tropical western North Pacific

## 1 Introduction

The intraseasonal oscillation (ISO) is an important component of climate variability in the tropical Indo-Pacific region. The ISOs determine the wet and dry spells in the rainy season (Mao and Chan 2005; Kulkarni et al. 2011), affect the onset of the summer monsoon in the South China Sea (Wu and Wang 2001; Wu 2010), and modulate the tropical cyclone activity over the western North Pacific and the South China Sea (Huang et al. 2011; Feng et al. 2013). The northward propagating intraseasonal oscillations may contribute to summer rainfall in southern China (Zhang et al. 2009; Chen et al. 2015). Unraveling the year-to-year variations in the source, propagation, and intensity of ISOs and the plausible factors is important for understanding the changes in the ISO impacts. In the present study, we are mainly concerned with changes in the intensity of ISOs over the tropical western North Pacific.

The ISO intensity change is connected to the seasonal mean change. This connection has two folds. One fold of

---

This paper is a contribution to the special issue on East Asian Climate under Global Warming: Understanding and Projection, consisting of papers from the East Asian Climate (EAC) community and the 13th EAC International Workshop in Beijing, China on 24–25 March 2016, and coordinated by Jianping Li, Huang-Hsiung Hsu, Wei-Chyung Wang, Kyung-Ja Ha, Tim Li, and Akio Kitoh.

✉ Renguang Wu  
renguang@mail.iap.ac.cn

<sup>1</sup> Center for Monsoon System Research, Institute of Atmospheric Physics, Chinese Academy of Sciences, Building 40, Huayanli, Beichen West Road, Chaoyang District, Beijing 100029, China

<sup>2</sup> State Key Laboratory of Numerical Modeling for Atmospheric Sciences and Geophysical Fluid Dynamics, Institute of Atmospheric Physics, Chinese Academy of Sciences, Beijing, China

this connection is the effect of the seasonal mean change on the ISO intensity by modulating the background. El Niño–Southern Oscillation (ENSO) has been indicated to be an important factor in the ISO intensity change due to its modulation of the seasonal mean background in the tropical Indo-Pacific region (Zhang and Gottschalck 2002; Teng and Wang 2003; Tam and Lau 2005; Hendon et al. 2007; Tang and Yu 2008; Gushchina and Dewitte 2012; Feng et al. 2015; Chen et al. 2016; Liu et al. 2016a, b). Previous studies showed an enhancement of the Madden–Julian Oscillation (MJO) activity over the equatorial western Pacific during the pre-developing and developing phases (Teng and Wang 2003; Hendon et al. 2007; Gushchina and Dewitte 2012; Chen et al. 2016), but a suppression of the MJO activity during the mature and decaying phases of the eastern Pacific El Niño (Tam and Lau 2005; Chen et al. 2016). The MJO activity is strengthened over the equatorial central Pacific during the mature and decaying phases of the central Pacific El Niño (Gushchina and Dewitte 2012; Chen et al. 2016).

Over the western North Pacific where the largest ISO variance is observed in boreal summer, the 15–40-day ISO is intensified during July–October in El Niño developing years (Teng and Wang 2003). Liu et al. (2016a) noted that the eastern Pacific cooling induces large intensification of 30–90-day intraseasonal variability there in boreal summer. Liu et al. (2016b) showed that the boreal summer ISO over the western North Pacific is dominated by a higher-frequency oscillation with a period of 20–40 days in the El Niño years, but by a lower-frequency oscillation with a period of 40–70 days during the La Niña years. Kajikawa and Yasunari (2005) and Yang et al. (2008) identified an enhanced 12–25-day intraseasonal oscillation over the South China Sea during the early summer corresponding to enhanced equatorial central Pacific convection. These previous studies are mainly confined to the ISO intensity changes during boreal summer. The ENSO-related circulation anomaly pattern evolves with season (Wu et al. 2003). As such, the ENSO-induced seasonal mean change may vary with the phase of ENSO. Thus, the modulation of ISOs by ENSO may occur in difference regions during other seasons. However, where the ISO is modulated during other seasons is not well addressed.

The other fold of the ISO–seasonal mean connection is the feedback of ISO on the seasonal mean. The impacts of the MJO activity over the equatorial western Pacific on ENSO have been studied in previous studies (see review of Zhang 2005 and Zhang 2013). The ISO feedback on local seasonal mean SST anomaly in the tropical western North Pacific during boreal summer is suggested by Wu and Cao (2016). They speculate that the feedback is related to the asymmetry of surface heat flux perturbations induced by ISOs. The surface latent heat flux anomalies due to ISOs

may be larger in the active phase than in the inactive phase (with opposite signs) due to the nonlinear effects of wind speed. This leads to net ISO-induced seasonal mean latent heat flux anomalies that may contribute to seasonal mean SST anomalies. In this study, we perform further analysis to demonstrate the ISO-induced latent heat flux effects in seasonal mean SST anomalies in the tropical western North Pacific.

Thus, in the present study, we address two issues: (1) The factors for the ISO intensity change over the tropical western North Pacific during boreal spring through fall and (2) The feedback of ISO intensity change on seasonal mean SST in the tropical western North Pacific. The organization of the rest of the text is as follows. In Sect. 2, we describe the datasets used in the present study and the methods used to decompose the surface latent heat flux. We present a local correlation analysis between the ISO intensity and SST change during different seasons in Sect. 3. In Sect. 4, we analyze the factors for the ISO intensity change over the western North Pacific. In Sect. 5, we focus on demonstrating the feedback of the ISO intensity change on seasonal mean SST change. A summary is presented in Sect. 6.

## 2 Data and methods

### 2.1 Datasets

The National Centers for Environmental Prediction–Department of Energy (NCEP–DOE) reanalysis 2 (Kanamitsu et al. 2002) provides the following variables: daily means of winds at 850 hPa, surface (10 m) winds, surface (2 m) specific humidity, and surface skin temperature and monthly means of winds at 850 and 200 hPa, vertical p-velocity at 500 hPa, surface (2 m) specific humidity, total cloud cover, and surface heat fluxes (shortwave radiation, longwave radiation, latent heat flux, and sensible heat flux). The surface variables (surface heat fluxes, cloud cover, surface wind, surface specific humidity, and surface skin temperature) are on T62 Gaussian grids. The other variables are on  $2.5^\circ \times 2.5^\circ$  grids. The reanalysis variables cover the time period starting from January 1979 and are obtained from <ftp://ftp.cdc.noaa.gov/>. The convention of surface heat fluxes is positive for downward shortwave radiation (SWR) and for upward longwave radiation (LWR), latent heat flux (LHF), and sensible heat flux (SHF).

The present study uses monthly mean sea surface temperature (SST) of the National Oceanic and Atmospheric Administration (NOAA) optimum interpolation (OI) version 2 (Reynolds et al. 2002). This SST dataset is on a  $1^\circ \times 1^\circ$  grid and covers the period from December 1981 to present. The OI SST is provided by the NOAA/OAR/ESRL PSD, Boulder, Colorado, USA and available at <http://www.>

[esrl.noaa.gov/psd/](http://esrl.noaa.gov/psd/). The SST tendency at a specific month is calculated as the difference of SST in the succeeding month minus that in the preceding month, divided by 2.

The present study uses monthly mean oceanic current and temperature from the Geophysical Fluid Dynamics Laboratory (GFDL) ocean data assimilation product (Griffies et al. 2004). The product has 50 vertical levels with 22 levels of 10-m thickness each in the top 220 m. The longitudinal resolution is 1° and the meridional resolution varies from about 1/3° near the equator to 1° at 30° latitude. This product is available from 1979 to 2007.

The mixed layer depth used in the present study is based on monthly mean climatology of de Boyer Montégut et al. (2004). This mixed layer depth climatology is produced by an objective analysis of available vertical profiles from 1941 to 2002. A threshold value of a temperature difference of 0.2 °C is used in determining the mixed-layer depth. This data set is one a 2° × 2° grid.

### 2.2 ISO intensity

In the present study, the intensity of the ISOs is measured by the kinetic energy of intraseasonal variations of winds at 850 hPa, following previous studies (Chen et al. 2016; Wu and Cao 2016). A comparison shows that the kinetic energy based ISO intensity tends to be consistent with that based on the squared root of intraseasonal outgoing long-wave radiation (OLR) variance (Wu and Cao 2016). As the ISOs have two profound periods: 10–20 day and 30–60 day (Chen and Chen 1995; Fukutomi and Yasunari 1999; Annamalai and Slingo 2001; Kajikawa and Yasunari 2005; Mao and Chan 2005; Kikuchi and Wang 2009), we separate the ISOs in the 10–20-day and 30–60-day time bands. Following Wu (2010) and Wu et al. (2015), we use a 9-day running mean minus a 21-day running mean to obtain the 10–20-day ISOs and a 29-day running mean minus a 61-day running mean to obtain the 30–60-day ISOs. The kinetic energy is calculated for the above two ISOs, respectively, for boreal winter (December–January–February, DJF for brevity), spring (March–April–May, MAM for brevity), summer (June–July–August, JJA for brevity), and fall (September–October–November, SON for brevity). The average values of the kinetic energy during a specific season represent the intensity of ISOs in that season.

### 2.3 Decomposition of surface latent heat flux

An individual variable may be considered to consist of variations on different time scales. We consider three components: climatological mean, the interannual variation with periods over 91-days, and the high-frequency variation with periods shorter than (including) 90-days. Further, the high-frequency variation includes 10–20-day and 30–60-day

ISOs. Here, we use subscript “clim”, “int”, “high”, and “1” to represent the climatological mean, interannual variation, high-frequency variation, and 10–20-day ISO, respectively. The SST, wind vector, and specific humidity can be written as follows:

$$SST = SST_{clim} + SST_{int} + SST_{high},$$

$$\vec{V} = \vec{V}_{clim} + \vec{V}_{int} + \vec{V}_{high},$$

$$q_a = q_{a_{clim}} + q_{a_{int}} + q_{a_{high}}.$$

For surface latent heat flux, we obtain different components in the following ways. We replace total wind, SST, specific humidity in the formula of calculating latent heat flux with the sum of climatological mean and interannual variation of wind, SST, specific humidity to calculate the interannual component (including climatological mean variation) of latent heat flux. The difference between the total and the interannual component is used to represent the high-frequency component of latent heat flux. Physically, the above difference is attributed to the contribution of high-frequency wind, SST, and specific humidity variations. According to above, the total, interannual component, and high-frequency component of latent heat flux can be written as follows:

$$LHF = \rho_a C_e L \left| \vec{V} \right| [q_s(SST) - q_a],$$

$$LHF_{int} = \rho_a C_e L \left| \vec{V}_{clim} + \vec{V}_{int} \right| [q_s(SST_{clim} + SST_{int}) - (q_{a_{clim}} + q_{a_{int}})],$$

$$LHF_{high} = LHF - LHF_{int},$$

where  $\rho_a$  is the surface air density,  $C_e$  is the latent heat exchange coefficient,  $L$  is the latent heat of vaporization, and  $q_s$  is the saturation specific humidity at SST.

To obtain the 10–20-day ISO component of latent heat flux, we first subtract the 10–20-day ISO components from the total wind, SST, and specific humidity to calculate the latent heat flux (denoted as  $LHF'_1$ ). The difference between the total and the above-calculated latent heat flux is attributed to the 10–20-day intraseasonal variations of wind, SST, and specific humidity and thus it represents the contribution of the 10–20-day ISO to latent heat flux (denoted as  $LHF_1$ ). The formulas to calculate the 10–20-day intraseasonal component of latent heat flux are as follows:

$$LHF'_1 = \rho_a C_e L \left| \vec{V} - \vec{V}_1 \right| [q_s(SST - SST_1) - (q_a - q_{a_1})],$$

$$LHF_1 = LHF - LHF'_1.$$

Our way of decomposing surface latent heat flux due to variations on different time scales is different from the time filtering corresponding to different time bands. As the component due to high-frequency variations may accumulate to contribute to low-frequency component, the time filtering cannot separate properly the contributions due to variations of wind, SST, and specific humidity on different time scales. Our method based on physical consideration can reveal reasonably the contribution of high-frequency variations to seasonal mean component of latent heat flux.

The above method may be applied to sensible heat flux and radiation fluxes as well in principle. In this study, we restrict the decomposition to latent heat flux for the purpose of illustration. Latent heat flux is a term that involves calculation of both saturation specific humidity and wind speed that are nonlinearly dependent upon SST and wind vector, respectively. Latent heat flux is also a major surface heat flux term over the tropical oceans.

### 3 Local relationship between ISO intensity and SST change

In this section, we present an analysis of local correlation of the ISO intensity with seasonal mean SST and SST tendency to motivate the readers. The correlation is calculated for the four seasons separately to unravel the seasonal dependence of the relation. Such correlation helps to reveal local relationship (Wu et al. 2006; Wu and Kirtman 2007), but it has limitation in providing information about the influence of remote forcing. A positive ISO intensity-SST correlation denotes that a higher SST corresponds to a stronger ISO activity. Higher SST may induce lower-level moisture convergence (Lindzen and Nigam 1987) and anomalous cyclonic winds and ascent (Gill 1980). Such large-scale background field change is favorable for a stronger ISO activity (Teng and Wang 2003; Chen et al. 2016; Liu et al. 2016a; Wu and Cao 2016). On the contrary, lower SST may lead to large-scale background field change that suppresses the ISO activity. This local SST effect on the ISO activity in the equatorial western-central Pacific has been demonstrated by previous studies (e.g., Chen et al. 2016; Liu et al. 2016a). Thus, a positive ISO intensity-SST correlation may indicate that local SST anomaly plays a role in modulating the ISO activity. A negative correlation of ISO intensity-SST tendency denotes that a stronger ISO activity is accompanied by a SST decrease. A stronger ISO is accompanied by larger fluctuations in surface winds. Due to the nonlinear dependence of surface latent heat flux on surface wind speed change, this may lead to a net heat loss of the ocean via surface latent heat flux, resulting a net effect of SST cooling. This suggests a plausible feedback of the ISO intensity on seasonal mean SST change. Thus,

the distribution of the above correlations provides useful information about where the SST change may influence the atmospheric ISO activity in situ and where the ISO intensity may feedback on local seasonal SST change. We analyze the local correlation for the 10–20-day and 30–60-day ISOs separately in view of the scale dependence of the ISO-SST relationship (Wu et al. 2015; Ye and Wu 2015; Cao et al. 2016).

The local correlation of the 10–20-day ISO intensity and SST displays positive correlation in the tropical central and eastern Pacific in all the four seasons. The location and magnitude of the positive correlation shows some differences among the four seasons. In winter, large positive correlation covers the tropical central Pacific (Fig. 1a). In spring, large positive correlation extends to the equatorial eastern Pacific (Fig. 1b). In summer, large positive correlation is mainly confined to the central North Pacific (Fig. 1c). In fall, large positive correlation extends to the subtropical southeastern Pacific (Fig. 1d). In summer and fall, large positive correlation is observed in the tropical southeastern Indian Ocean (Fig. 1c, d). In winter, positive correlation is present in the subtropical southeastern Indian Ocean (Fig. 1a). The local correlation of the 30–60-day ISO intensity and SST tends to display a similar distribution in the four seasons, but with a smaller magnitude in general (figures not shown). The above results indicate that the tropical central Pacific in the four seasons and the tropical southeastern Indian Ocean in summer and fall are two regions where local SST anomaly may play a role in modulating in situ ISO intensity.

The point-wise correlation of the 10–20-day ISO intensity and the SST tendency displays an obvious seasonal change. Here, we mainly pay attention to the negative correlation with enhanced ISO activity corresponding to the SST decrease. In winter, large negative correlation is observed in the tropical southeastern Indian Ocean and the tropical southwestern Pacific Ocean (Fig. 2a). In spring, large negative correlation is located in the eastern South China Sea and the Philippine Sea, and the tropical South Pacific Ocean (Fig. 2b). In summer, very large negative correlation is observed in the tropical western North Pacific with the center correlation reaching  $-0.7$  (Fig. 2c). In fall, large negative correlation is observed in the tropical western North Pacific and central-southern South China Sea (Fig. 2d). The point-wise correlation of the 30–60-day ISO intensity and the SST tendency displays negative correlation in the above regions as well, but with a reduced magnitude in general except for spring when the negative correlation in the Philippine Sea is somewhat larger (figures not shown). The above results indicate that the tropical western North Pacific in spring through fall is a preferred region for a plausible feedback of the ISO intensity on seasonal mean SST change. In the following analysis, we will focus on

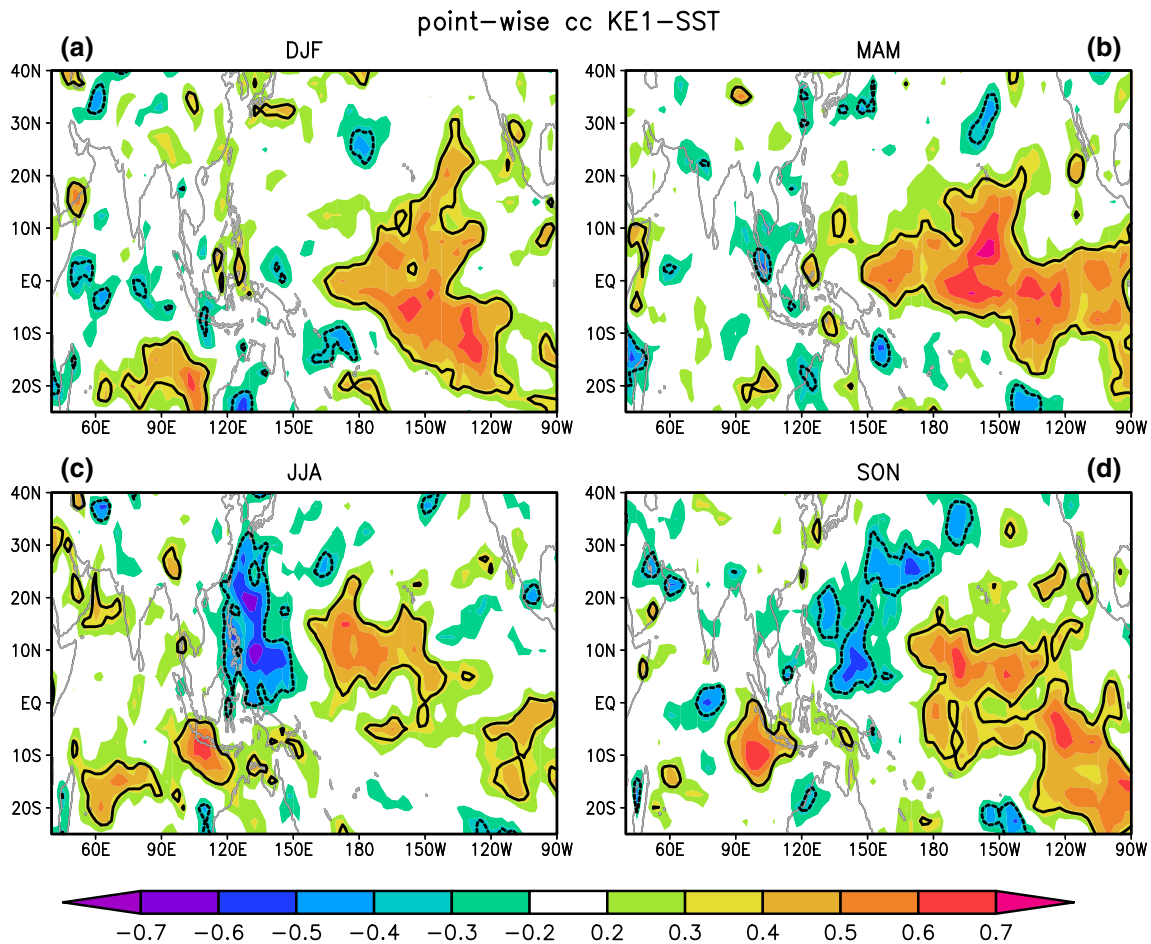


**Fig. 1** The point-wise and simultaneous correlation of the seasonal mean 10–20-day ISO intensity (KE1) and SST for the period 1982–2014. **a** DJF, **b** MAM, **c** JJA, and **d** SON. The *thick lines* denote

regions where the correlation is significant at the 95 % confidence according to the Student *t* test

documenting the factors for and feedback of the ISO intensity change in this region during spring, summer, and fall.

To demonstrate the relationship of the ISO intensity and SST changes, we calculate the lead-lag correlation of area-mean monthly SST anomaly with respect to area-mean seasonal ISO intensity. In view of the location change with season, we select different regions for spring, summer, and fall based on the location of large negative correlation. The selected regions for the 10–20-day ISOs are, respectively, 5°–15°N, 115°–135°E for spring, 5°–15°N, 130°–160°E for summer, and 12.5°–22.5°N, 140°–180°E for fall. The locations of these regions are denoted in Fig. 2b–d. A pronounced drop in the SST correlation is apparent in all the three regions with respect to an increase in the ISO intensity (Fig. 3). For summer, the drop occurs from June to August. For spring, the drop is observed from April to June. For fall, the drop occurs from September to November. The change in the correlation coefficient is large, reaching 0.8 in all the three cases. We also calculate the lead-lag

correlation of monthly SST with respect to the 30–60-day ISO intensity with the area averages determined based on the locations of large negative 30–60-day ISO intensity–SST tendency. A similar drop of correlation is observed (Figure not shown). In comparison, both the range of drop and the magnitude of the negative correlation after the drop are smaller compared to the 10–20-day ISO. This suggests that the feedback of the 10–20-day ISO intensity change on SST change is larger than that of the 30–60-day ISO intensity, which is consistent with Wu and Cao (2016) for summer. In the following, we only analyze the 10–20-day ISO intensity change.

#### 4 Factors for changes in the 10–20-day ISO intensity

In this section, we analyze the seasonal mean anomalies corresponding to the 10–20-day ISO intensity change

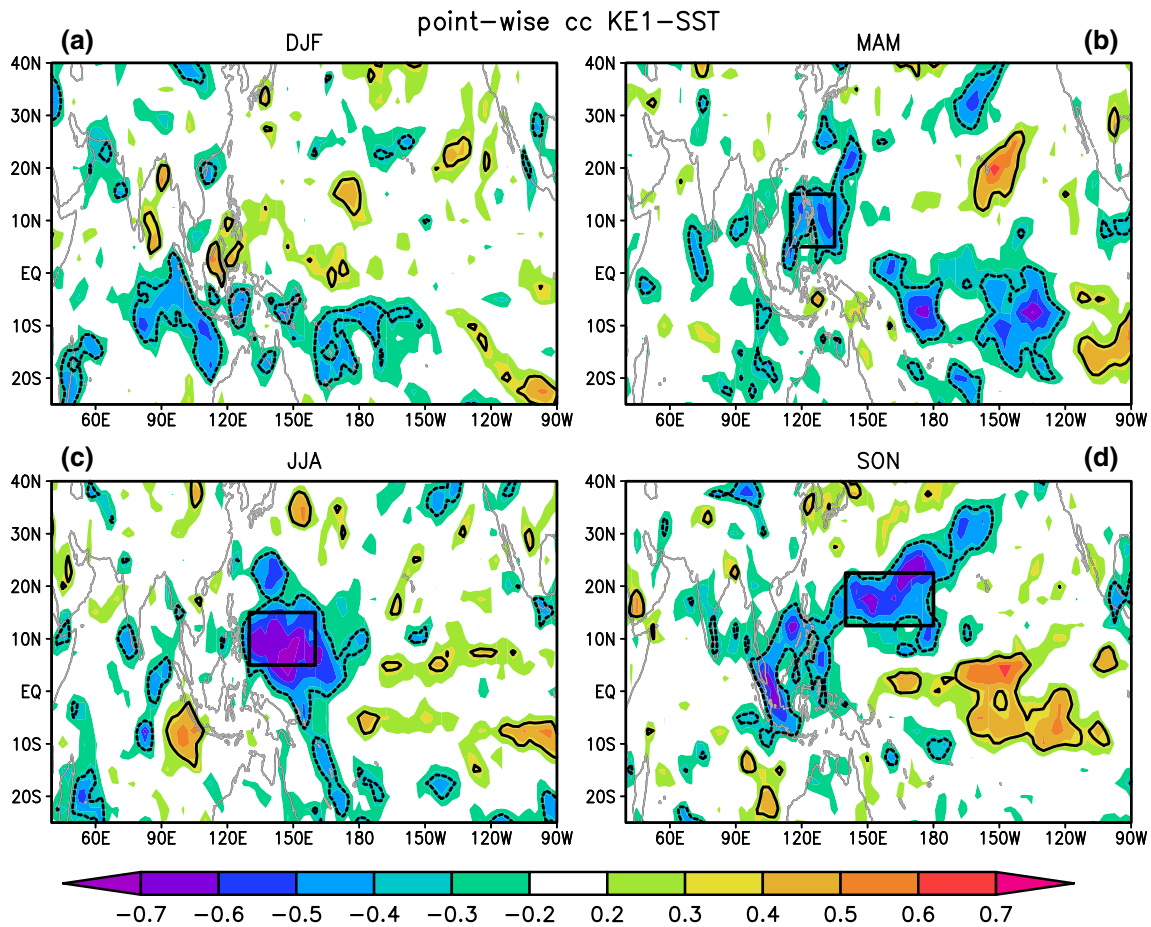


**Fig. 2** Similar to Fig. 1 except for the SST tendency. The *boxes* in Fig. 2b–d denote the regions for area averaging of the 10–20-day ISO intensity

**Fig. 3** Lead-lag correlation of area-mean monthly mean SST with respect to area-mean 10–20-day ISO intensity (KE1) averaged in the region of 5°–15°N and 130°–160°E in JJA (*solid-red line*), 5°–15°N and 115°–135°E in MAM (*dash-green line*), and 12.5°–22.5°N and 140°–180°E in SON (*dot-blue line*). Refer to Fig. 2b–d for locations of these regions. The *red, green, and blue vertical lines* denote the reference 10–20-day ISO intensity time in JJA, MAM, and SON, respectively

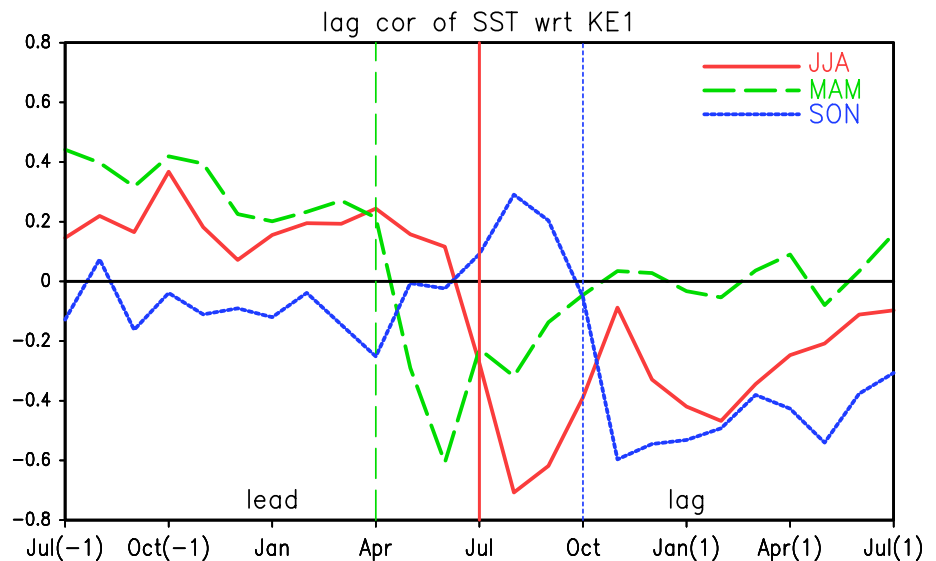
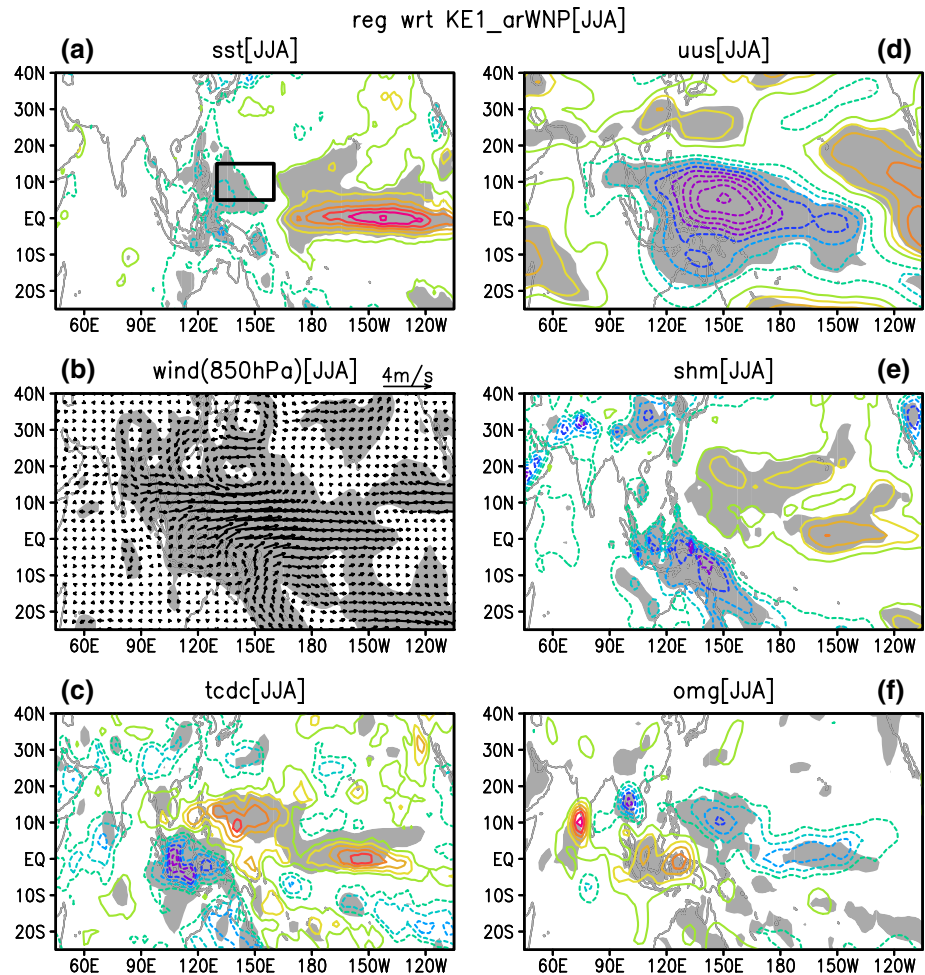


**Fig. 4** Simultaneous regression with respect to normalized JJA 10–20-day ISO intensity (KE1) averaged in the region of 5°–15°N and 130°–160°E (the box in a) for the period 1982–2014. **a** SST (°C, interval: 0.1 °C), **b** 850 hPa wind (m/s, scale at the top-right), **c** total cloud amount (%), **d** vertical shear of zonal wind (m/s, interval: 0.5 m/s), **e** surface specific humidity (g/kg, interval: 0.1 g/kg), and **f** 500 hPa vertical  $p$ -velocity (0.01 Pa/s, interval  $0.5 \times 0.01$  Pa/s). The zero contours have been suppressed. Shading denotes that the anomalies are significant at the 95 % confidence level according to the Student  $t$  test



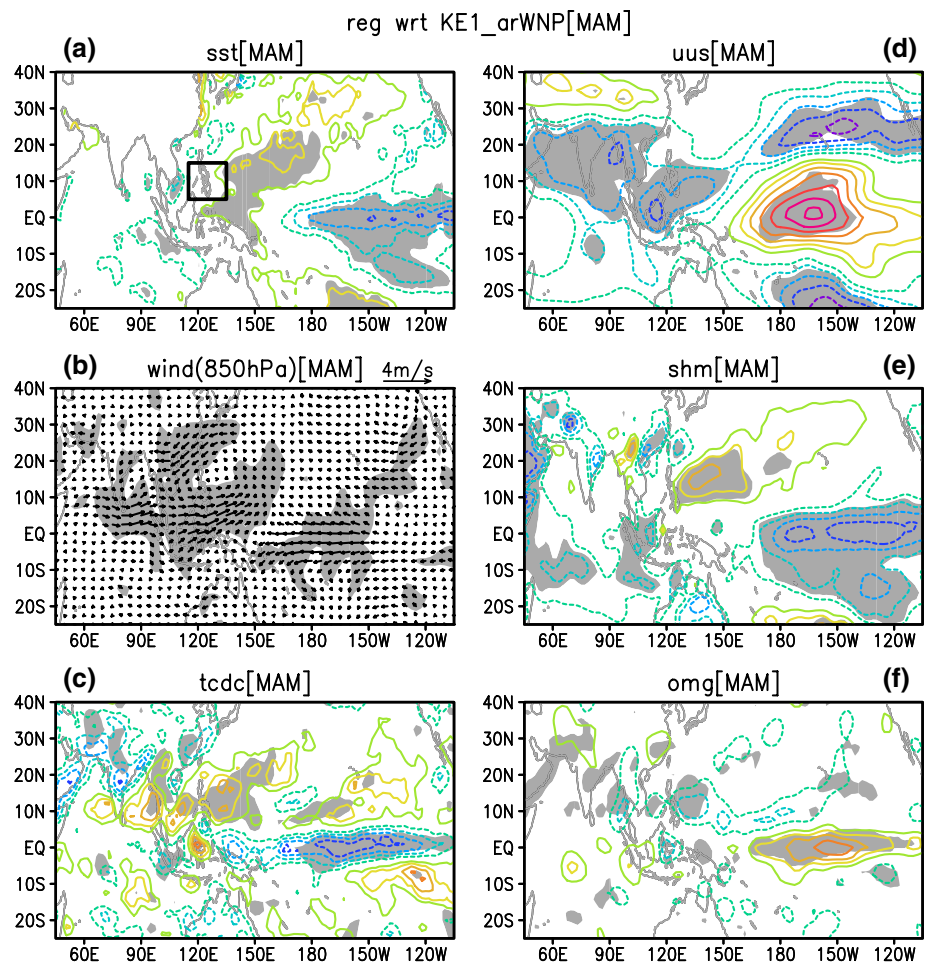
averaged over the regions where large negative ISO intensity–SST tendency correlation is detected (Fig. 2). Such analysis not only helps to reveal the factors for the ISO intensity change, but also provide useful information for understanding the difference in the distribution of latent heat flux anomalies on different time scales. The latter is necessary for addressing the feedback of the ISO intensity change on seasonal SST anomalies in the next section. We present the analysis in summer first for which the ISO intensity change has been documented in previous studies, and then that in spring and fall for which few studies have been made.

In summer, corresponding to the enhanced 10–20-day ISOs over the tropical western North Pacific, local SST anomalies are small or negative (Fig. 4a). This confirms that local SST anomaly does not contribute to the ISO intensity change. Large positive SST anomalies are observed in the equatorial central-eastern Pacific. The lower-level wind anomalies feature a Rossby wave type response to positive SST anomalies in the equatorial central-eastern Pacific, with large anomalous cyclones over

the western North and South Pacific and large anomalous westerly winds along the equatorial western-central Pacific (Fig. 4b). This contributes to negative anomalies in vertical shear of zonal winds over the tropical western-central Pacific (Fig. 4d). Consistently, there are more cloud cover and anomalous upward motion extending from the equatorial central Pacific northwestward to the tropical western North Pacific (Fig. 4c, f). The surface humidity increases over the equatorial central-eastern Pacific and the tropical North Pacific (Fig. 4e). The above seasonal mean anomalies are favorable for strengthening the ISO activity over the tropical western North Pacific, consistent with previous studies (Teng and Wang 2003; Yang et al. 2008; Liu et al. 2016a; Wu and Cao 2016).

In spring, corresponding to the enhanced 10–20-day ISOs around the Philippines, significant negative and positive SST anomalies are observed in the equatorial central-eastern Pacific and the subtropical central North Pacific, respectively (Fig. 5a). Lower-level anomalous winds feature diverging easterly over the equatorial

**Fig. 5** Similar to Fig. 4 except for MAM and the region of 5°–15°N and 115°–135°E



central Pacific and a large cyclone over the western North Pacific through the Bay of Bengal (Fig. 5b). Consistently, more cloud cover and anomalous upward motion cover the tropical western North Pacific through the Bay of Bengal and less cloud cover and anomalous downward motion control the equatorial central-eastern Pacific (Fig. 5c, f). The atmospheric changes over the tropical western North Pacific are contributed by both remote forcing of the equatorial central Pacific SST anomalies and the effect of SST anomalies in the western North Pacific (Wu and Wang 2000). The local SST anomalies also contribute to the increase in lower-level moisture (Fig. 5e) (Wu and Wang 2000). The vertical shear of zonal winds displays significant negative anomalies in the region extending from the tropical western North Pacific to the South Asia (Fig. 5d). Overall, the easterly vertical shear, the enhanced lower-level humidity, and upward motion are all favorable for enhancing the ISO activity over the tropical western North Pacific.

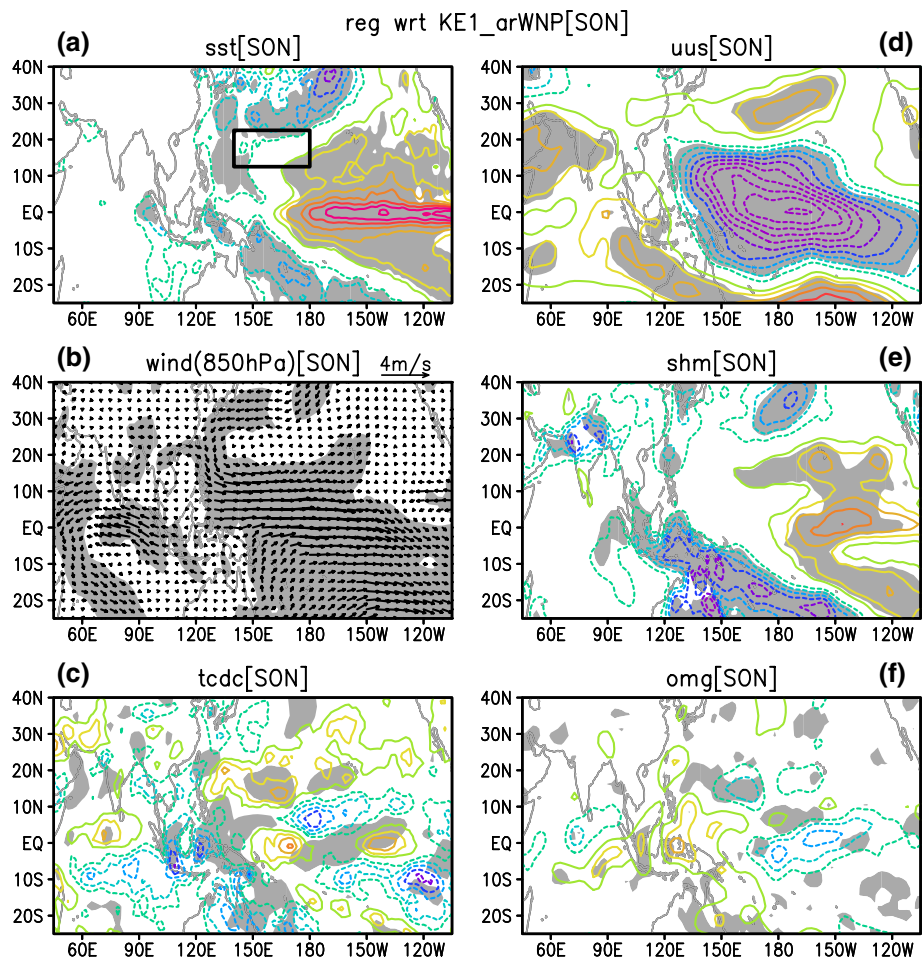
In fall, enhanced 10–20-day ISOs over the western North Pacific occur in a region of transition between positive and

negative SST anomalies (Fig. 6a). Negative SST anomalies are located to the west flank and north of the concerned region and large positive SST anomalies are observed in the equatorial central-eastern Pacific. The lower-level wind anomalies feature a Rossby wave type response to the SST anomalies in the equatorial central-eastern Pacific with large anomalous cyclones covering the tropical North and South Pacific and strong westerlies over the equatorial western-central Pacific (Fig. 6b). Large easterly vertical shear of zonal winds controls the tropical western-central Pacific (Fig. 6d). The surface humidity increase is limited to the tropical eastern Pacific (Fig. 6e). More cloud cover and anomalous upward motion are observed over the tropical western North Pacific (Fig. 6c, f). The easterly vertical shear and anomalous lower-level convergence and upward motion appear to be the main factors for enhanced ISO activity over the western North Pacific.

Comparing the SST anomalies in the three seasons, the distribution in summer and fall corresponds to the developing El Niño, whereas that in spring features the decaying La Niña phase. This suggests that the 10–20-day ISO intensity



**Fig. 6** Similar to Fig. 4 except for SON and the region of 12.5°–22.5°N and 140°–180°E



change is related to the phase of ENSO. In addition, the change in the location of large ISO intensity indicates that the modulation of ENSO on the ISO intensity occurs in different regions. The above relationship appears to be consistent with the evolving anomalies associated with ENSO. The ENSO-related atmospheric anomalies over the western North Pacific move eastward with the ENSO phase (Wu et al. 2003). As such, the background fields of the ISOs are subject to modulation in different regions during different phases of ENSO. This explains why the ISO intensity change is observed in different locations during different seasons.

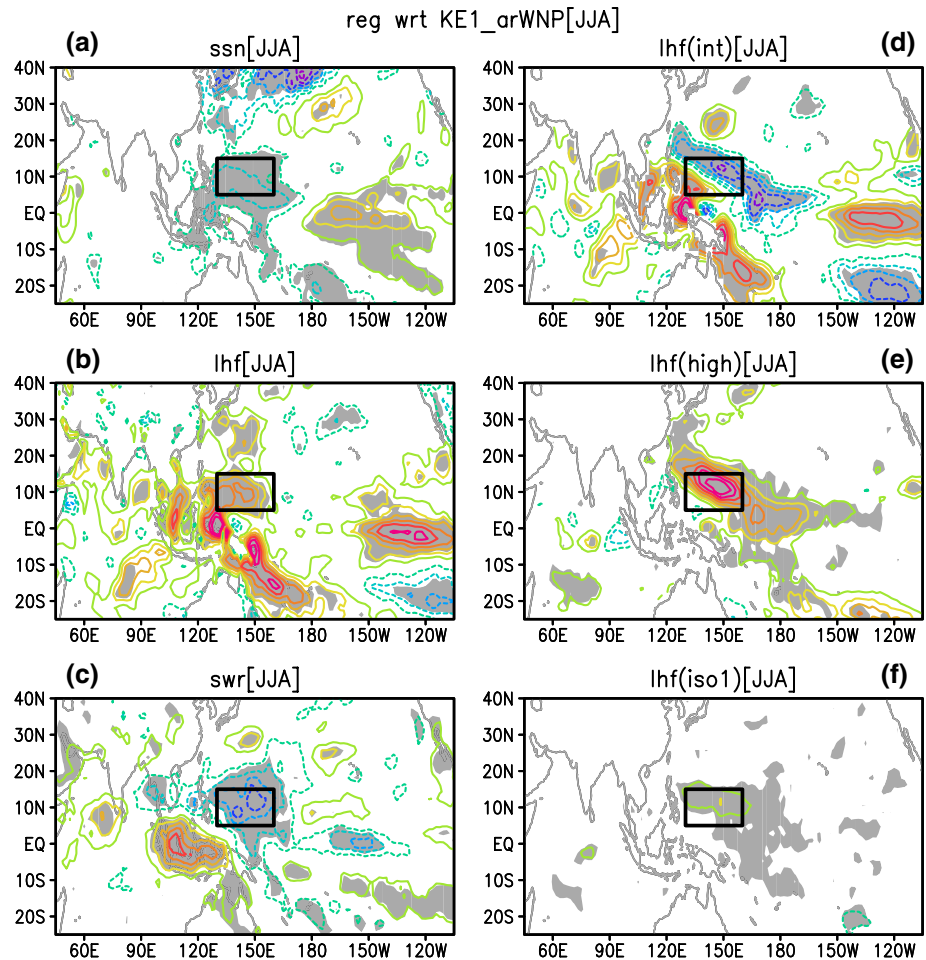
## 5 Feedback of the 10–20-day ISO intensity on seasonal mean SST change

In this section, we diagnose the contribution of different surface heat flux terms to the SST tendency. Over the tropical oceans, shortwave radiation and latent heat flux are the two major terms. The longwave radiation anomalies are smaller

than the shortwave radiation anomalies. The sensible heat flux anomalies are smaller than the latent heat flux anomalies. Thus, we only show maps of shortwave radiation and latent heat flux anomalies. The box-mean values of all the four terms will be compared in the last. As in Sect. 4, we present the analysis in summer first, followed by that in spring and fall.

In summer, the enhanced 10–20-day ISO over the tropical western North Pacific is accompanied by significant negative SST tendency (Fig. 7a). The SST tendency is contributed by an increase in upward latent heat flux (Fig. 7b) and a decrease in downward shortwave radiation (Fig. 7c). The shortwave radiation decrease is consistent with increase in cloud cover and upward motion (Fig. 4c, f). The latent heat flux increase in the southwestern part may be explained by anomalous seasonal mean westerly winds (Fig. 4b) that increase seasonal mean wind speed as the anomalous winds are in the same direction as climatological mean winds (Figs. 4b, 8b). However, the latent heat flux increase in the northeastern part cannot be explained by seasonal mean wind anomalies that are against climatological easterly winds and thus lead to a decrease in

**Fig. 7** Simultaneous regression with respect to normalized JJA 10–20-day ISO intensity (KE1) in the region of 5°–15°N and 130°–160°E (the *boxes*) for the period 1982–2014. **a** SST tendency converted to the unit of heat flux using a mixed-layer depth of 45 m, **b** latent heat flux, **c** net shortwave radiation, **d** interannual component of latent heat flux, **e** high-frequency component of latent heat flux, and **f** 10–20-day component of latent heat flux. The contour interval is  $3 \text{ W/m}^2$ . The zero contours have been suppressed. *Shading* denotes that the anomalies are significant at the 95 % confidence level according to the Student *t* test



seasonal mean wind speed. This is clearly demonstrated by the distribution of interannual component of latent heat flux anomalies that displays a pronounced southwest-northeast contrast (Fig. 7d), which is consistent with the wind speed contrast. In comparison, the high-frequency component of latent heat flux anomalies displays a large increase in a northwest-southeast tilted band (Fig. 7e). The increase in the high-frequency component cancels the decrease in the interannual component, leading to an increase in total latent heat flux (Fig. 7b). The 10–20-day component of latent heat flux has a positive contribution in the region (Fig. 7f). The magnitude of the 10–20-day component is about 1/4 of the total anomalies, indicating a non-negligible contribution. We will come back to this point later.

In spring, the enhanced 10–20-day ISO around the Philippines is accompanied by significant negative SST tendency (Fig. 9a). The shortwave radiation has a major contribution to the SST tendency (Fig. 9c). The latent heat flux contribution appears small with opposite anomalies in the northern and southern parts (Fig. 9b). As anomalous westerly winds are against climatological easterly winds

(Figs. 5b, 8a), the seasonal mean wind speed effect leads to negative latent heat anomalies of the interannual component (Fig. 9d). The high-frequency component, however, has large positive anomalies (Fig. 9e), which tends to cancel the interannual component, leading to small total latent heat flux anomalies (Fig. 9b). The 10–20-day ISO has an important contribution to the SST tendency.

In fall, the enhanced 10–20-day ISO over the western North Pacific is accompanied by large negative SST tendency as well (Fig. 10a). The shortwave radiation has a large positive contribution to the SST tendency (Fig. 10c). The latent heat flux contribution is positive in the northern part, but negative in the southern part (Fig. 10b). The negative anomalies in the southern part where the anomalous winds are against climatological mean winds (Figs. 6b, 8c) are largely attributed to the interannual component (Fig. 10d), which is mostly cancelled by the high-frequency component (Fig. 10e). The positive anomalies in the northern part are due to the high-frequency component.

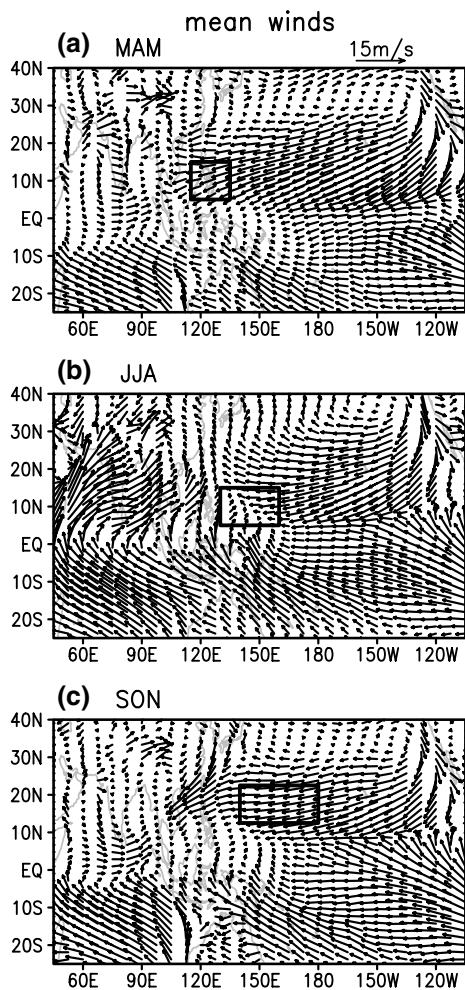


**Fig. 8** Climatological mean surface winds (m/s, scale at the *top-right*) in **a** MAM, **b** JJA, and **c** SON. The *boxes* denote the regions for area averaging of the 10–20-day ISO intensity in the respective season

The 10–20-day component has a positive contribution (Fig. 10f), with a magnitude about 1/3 of the high-frequency component.

For a quantitative comparison, we present in Table 1 the area-mean values averaged over the three regions for summer, spring, and fall. In summer, the shortwave radiation and latent heat flux contributions are comparable. The latent heat flux anomalies are dominated by the high-frequency component with the 10–20-day component contributing to about 1/4, comparable to the interannual component (with an opposite sign). The longwave radiation contribution is about 1/4 of shortwave radiation contribution with a cancelling effect. The sensible heat flux term is small. The total surface heat flux anomaly is much larger than the SST tendency.

In spring, the shortwave radiation contribution is a main one to the SST tendency. The interannual and

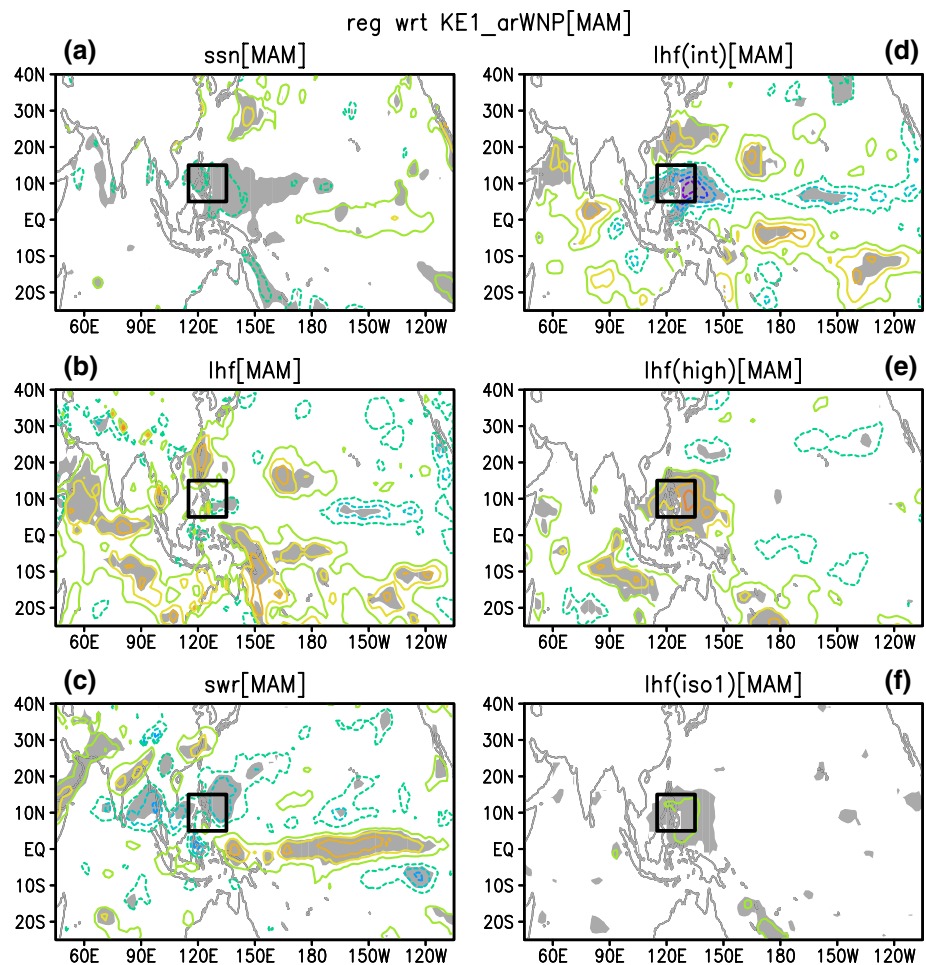
high-frequency components of latent heat flux anomalies tend to cancel with each other. The 10–20-day component of latent heat flux anomalies is comparable to the SST tendency and accounts for about 1/3 of the high-frequency component. The longwave radiation and sensible heat flux terms are small. The net surface heat flux is somewhat larger than the SST tendency.

In fall, the shortwave radiation contribution is larger than the latent heat flux contribution. The high-frequency component is larger than the interannual component of latent heat flux anomalies (with opposite sign). The 10–20-day component of latent heat flux anomalies is large, explaining more than 1/3 of the high-frequency component. The longwave radiation and sensible heat flux terms are small. The net heat flux anomaly is somewhat smaller than the SST tendency.

From the above analyses, the enhanced ISO activity induces an increase in high-frequency component of latent heat flux, which has an important contribution to the SST tendency. This validates the feedback of the ISO on the seasonal mean SST change. Another feature is that the high-frequency component tends to be opposite to the interannual component of latent heat flux. To further demonstrate the ISO impact on intraseasonal latent heat flux variations, we calculate local correlation between the 10–20-day ISO intensity and the 10–20-day component of the latent heat flux for spring, summer, and fall, respectively. The tropical western North Pacific appears as a region with the highest correlation in all the three seasons where the correlation coefficient is as high as 0.7 (Fig. 11). This indicates that the tropical western North Pacific is a preferred region for the ISO feedback on local seasonal mean SST change. High correlation is also observed in tropical southwestern Pacific in spring and fall (Fig. 11a, c). Another region with high correlation is the tropical southeastern Indian Ocean in summer and fall (Fig. 11b–c). Differently, the ISO activity in this region may be contributed by local SST anomaly (Fig. 1), whereas the ISO activity over the tropical western North Pacific is mainly due to remote forcing.

The accumulation of intraseasonal latent heat flux anomalies in the seasonal mean is due to the nonlinear dependence of latent heat flux variations on surface wind. This is demonstrated in Fig. 12 that is a scatter plot of area-mean surface zonal wind and surface latent heat flux in JJA averaged over the region of 5°–15°N, 130°–160°E where climatological mean winds are relatively weak (Fig. 8b). For both interannual and intraseasonal variations, the latent heat flux displays a nonlinear dependence upon surface wind. Larger latent heat flux is observed when there are large easterly and westerly wind anomalies. This is because both easterly and westerly wind anomalous increase surface wind speed and thus latent heat flux. In comparison, the interannual component is larger when there are easterly

**Fig. 9** Similar to Fig. 7 except for MAM in the region of 5°–15°N and 115°–135°E and using a mixed-layer depth of 30 m



wind anomalies (Fig. 12a), whereas the intraseasonal component is larger when there are westerly wind anomalies (Fig. 12b). For the intraseasonal variations, westerly and easterly winds correspond to active and inactive phases. Thus, the nonlinearity leads to a net seasonal mean anomaly of intraseasonal latent heat flux component.

The ISOs consist of wet and dry phases. One question is what are the respective effects of the dry and wet phases of the ISOs on seasonal mean SST change. For this purpose, the local dry and wet phases are determined based on local intraseasonal OLR anomalies. We first obtain the intraseasonal OLR anomalies. Then, the days with positive OLR anomalies are considered to belong to the dry phase and the days with negative OLR anomalies belong to the wet phase. Using our method of estimating the high-frequency component of latent heat fluxes, we calculate the accumulated latent heat flux anomalies corresponding to the wet and dry phases of the ISOs in the respective seasons. This is done for 10–90-day and 10–20-day ISOs respectively. Then, area-mean values of accumulated latent heat flux anomalies are obtained for the three concerned regions based on

regression on the regional mean 10–20-day ISO intensity. The results are shown in Table 2. From the Table, the latent heat flux anomalies averaged in the three regions are positive for both wet and dry phases, which are attributed to the nonlinear dependence of the latent heat flux upon surface wind. In comparison, the accumulated latent heat flux anomalies are much larger in the wet phase than in the dry phase in the region of summer for both the 10–90-day and 10–20-day ISOs and in the region of spring for the 10–90-day ISOs, comparable in the wet and dry phases in the region of spring for the 10–20-day ISOs, somewhat larger in the dry phase than in the wet phase in the region of fall for both the 10–90-day and 10–20-day ISOs.

## 6 Summary and discussions

An analysis of local correlation shows that the local SST impact on the 10–20-day ISO intensity is limited to the tropical central-eastern Pacific through the whole year and the tropical southeastern Indian Ocean in boreal summer and

**Fig. 10** Similar to Fig. 7 except for SON in the region of 12.5°–22.5°N and 140°–180°E and using a mixed-layer depth of 55 m

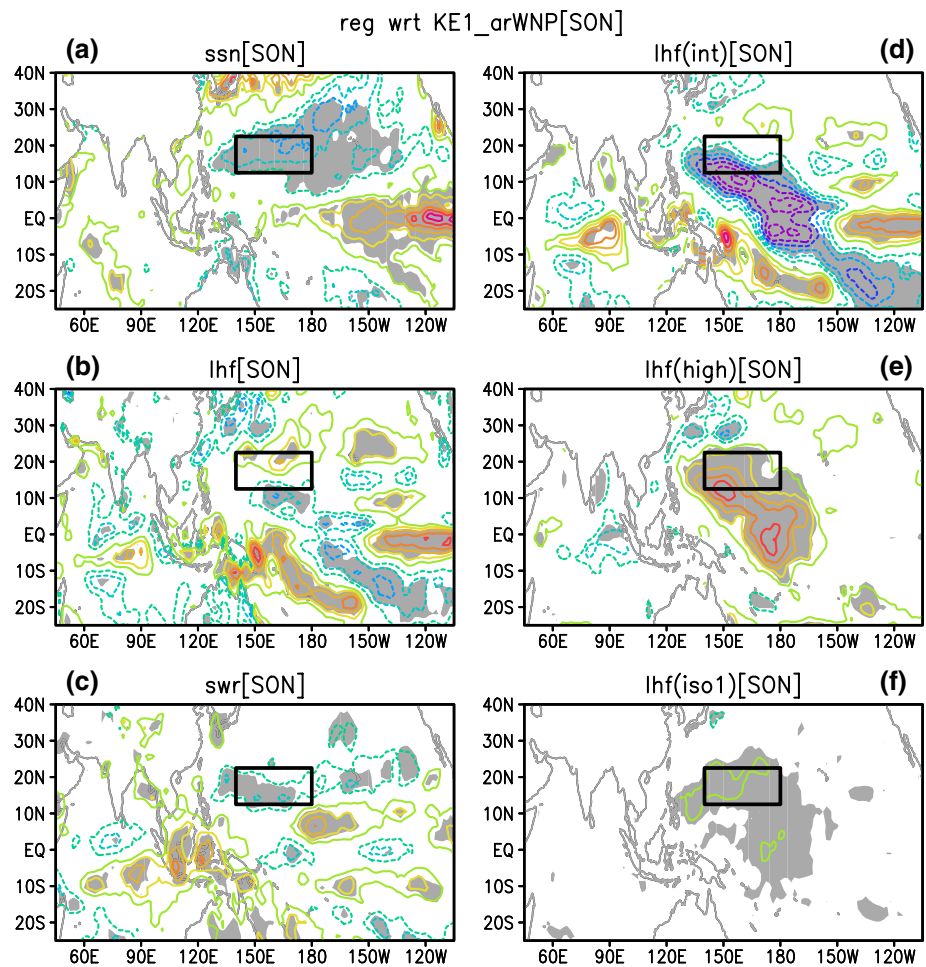


**Table 1** Area-mean values of SST tendency (SSTn), latent heat flux (lhf), the interannual component of latent heat flux (lhf(int)), the high-frequency component of latent heat flux (lhf(high)), the 10–20-day component of latent heat flux (lhf(iso1)), net shortwave radiation (swr), sensible heat flux (shf), net longwave radiation (lwr), net heat

flux (nhf), and the sum of ocean advection terms (adv) averaged over the region of 5°–15°N, 130°–160°E in JJA, 5°–15°N, 115°–135°E in MAM, and 12.5°–22.5°N, 140°–180°E in SON obtained by regression on 10–20-day ISO intensity in the same region and the same season

	SSTn	Lhf	Lhf (int)	Lhf (high)	Lhf (iso1)	Swr	Shf	Lwr	Nhf	Adv
JJA	−6.17	8.86	−3.73	12.58	3.00	−9.63	0.40	−2.36	−16.53	1.20
MAM	−3.62	0.54	−8.25	8.54	2.94	−4.13	−0.12	0.87	−3.68	0.25
SON	−7.00	1.63	−5.68	7.27	2.68	−3.71	0.19	−1.35	−4.18	0.15

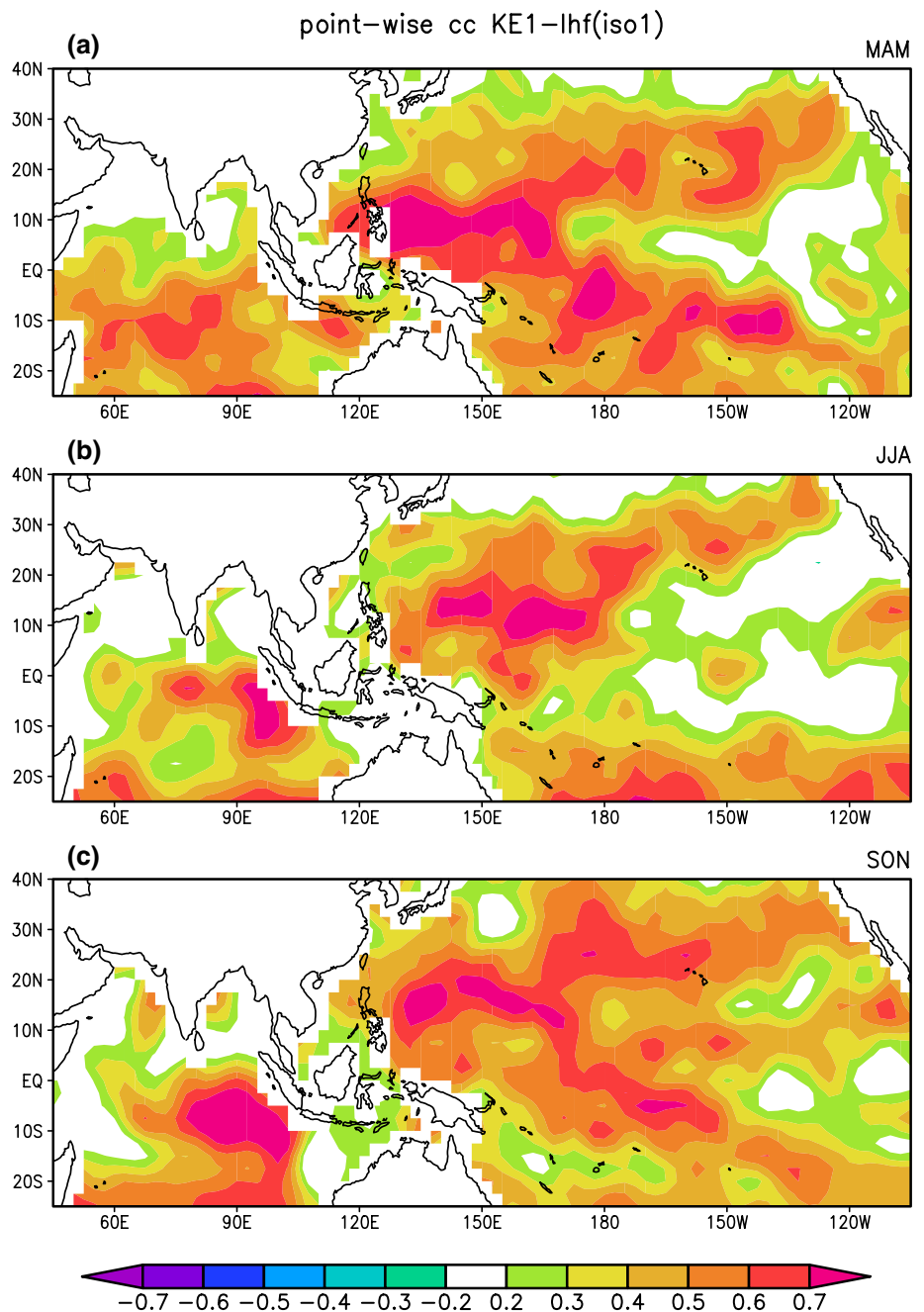
Refer to Fig. 2b–d for locations of these regions. The SST tendency has been converted to the unit of heat flux using a mixed-layer depth of 45 m in JJA, 30 m in MAM, and 55 m in SON based on de Boyer Montégut et al. (2004)’s mixed layer depth climatology. The unit is  $W/m^2$

fall. The 10–20-day ISO intensity is negatively correlated with seasonal mean SST tendency in the tropical western North Pacific during boreal spring, summer, and fall. The specific region of negative correlation changes with the season. The negative correlation indicates a plausible effect of the ISO intensity change on seasonal mean SST anomaly.

The 10–20-day ISO intensity change over the tropical western North Pacific is subject to influences of the

equatorial central-eastern Pacific SST anomalies during spring through fall. There is a supplementary contribution from the SST anomalies in the central North Pacific in spring. The influences of these SST anomalies are through modulating the vertical shear of zonal winds, lower-level moisture, and upward motion over the tropical western North Pacific. As the region of these background field changes induced by ENSO moves with the ENSO phase,

**Fig. 11** The point-wise and simultaneous correlation of the 10–20-day ISO intensity (KE1) and the 10–20-day component of latent heat flux anomalies for the period 1979–2014. **a** MAM, **b** JJA, and **c** SON



the specific location of the ISO intensity subject to most significant influence of ENSO displays a seasonal change.

Analysis shows that there is an important feedback of the 10–20-day ISO intensity over the tropical western North Pacific on local seasonal mean SST change. The feedback is through inducing accumulated ISO-induced latent heat flux anomalies in the seasonal mean. Such feedback is particularly prominent when the high-frequency component of latent heat flux anomalies overcomes the

interannual component (periods over 90-day). The 10–20-day intraseasonal component accounts for about 1/3 to 1/4 of the high-frequency (periods less than 90-day) latent heat flux anomalies over the tropical western North Pacific.

The feedback of ISOs on seasonal mean SST change is due to the nonlinear dependence of surface latent heat flux variations on surface winds. In the region of 5°–15°N, 130°–160°E where large high-frequency latent heat flux anomalies are detected (Fig. 7e), climatological mean

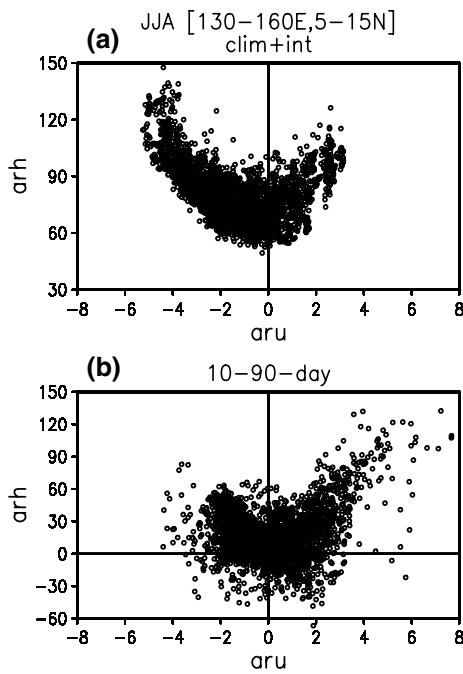


**Fig. 12** Scatter plot of area-mean surface zonal wind (aru) (m/s) and surface latent heat flux (arh) ( $W/m^2$ ) averaged over the region of  $5^{\circ}$ – $15^{\circ}$ N and  $130^{\circ}$ – $160^{\circ}$ E in JJA for the period 1982–2014. **a** climatological mean and interannual component, **b** 10–90-day component

winds are weak in boreal summer (Fig. 8b). Both the easterly winds in the inactive phase and the westerly winds in the active phase of the ISOs increase surface wind speed and thus latent heat flux. When averaged over the summer, there is a net anomaly of ISO-induced latent heat flux components, which may contribute to seasonal mean SST change.

The SST tendency and the surface heat flux contribution display differences in the three concerned regions. There are several plausible reasons for the differences. One is the effect of oceanic processes. The contribution of

oceanic horizontal and vertical advectons to the seasonal mean SST change has been estimated using monthly mean GFDL assimilation ocean current and temperature data. It turns out that the contribution of oceanic terms to the SST tendency is small in all the three regions (Table 1). Another plausible reason is the uncertainty of reanalysis surface heat fluxes. Previous studies indicate that the surface heat fluxes have large discrepancy among different products (e.g., Chou et al. 2004). The other reason is the use of a constant mixed layer depth in estimating the surface heat flux contribution to the SST tendency. In the active phase of the ISOs, the strong wind disturbances may lead to strong vertical mixing in the ocean upper-layer, leading to a deeper mixed layer depth. This would lead to a larger equivalent heat flux corresponding to the same SST tendency. Assuming a constant mixed layer depth may lead to an underestimation of the equivalent heat flux converted from the SST tendency. The intraseasonal wind fluctuations over the tropical western North Pacific tend to be larger in summer than in spring and fall, leading to a larger intraseasonal variation in the mixed layer depth. This may contribute to a larger difference between surface heat flux and SST tendency in summer than in spring and fall.

The present analysis is confined to the feedback of the ISO on seasonal mean SST via surface latent heat flux changes. Atmospheric intraseasonal oscillations are accompanied by intraseasonal variations in the ocean (Zhang 2005, 2013). These oceanic intraseasonal changes may contribute to seasonal mean SST anomaly through accumulation of atmospheric ISO-induced oceanic advection, upwelling, and mixing. Further analysis is needed for a quantitative estimation of relative contributions of various surface heat fluxes and oceanic processes on intraseasonal time scales to seasonal mean SST change. Another way of the ISO influence is the modulation of the oceanic mixed-layer depth. High temporal resolution oceanic data would be required for these analyses.

**Table 2** Area-mean values of anomalies of accumulated intraseasonal components of latent heat flux (lhf) in the dry phase, the wet phase, and both phrases of 10–90-day and 10–20-day ISOs averaged over the region of  $5^{\circ}$ – $15^{\circ}$ N,  $130^{\circ}$ – $160^{\circ}$ E in JJA,  $5^{\circ}$ – $15^{\circ}$ N,  $115^{\circ}$ – $135^{\circ}$ E

in MAM, and  $12.5^{\circ}$ – $22.5^{\circ}$ N,  $140^{\circ}$ – $180^{\circ}$ E in SON obtained by regression on 10–20-day ISO intensity in the same region and the same season

	10–90-day			10–20-day		
	Dry phase	Wet phase	Total	Dry phase	Wet phase	Total
JJA	1.66	4.76	6.42	0.38	2.61	3.00
MAM	1.35	3.16	4.51	1.96	2.04	3.10
SON	1.77	1.14	2.91	1.55	1.19	2.74

The unit is  $W/m^2$

**Acknowledgments** The two anonymous reviewers' comments help to improve the paper. This study is supported by the National Key Basic Research Program of China grant (2014CB953902), the National Key Research and Development Program grant (2016YFA0600603), and the National Natural Science Foundation of China grants (41475081, 41275081, and 41530425). The NCEP-DOE reanalysis 2 data and the NOAA OLR data were obtained from <ftp://ftp.cdc.noaa.gov/>. The NOAA OI version 2 SST data are obtained from <http://www.esrl.noaa.gov/psd/>.

## References

- Annamalai H, Slingo JM (2001) Active/break cycles: diagnosis of the intraseasonal variability of the Asian summer monsoon. *Clim Dyn* 18:85–102
- Cao X, Wu R, Chen SF (2016) Contrast of 10–20-day and 30–60-day intraseasonal SST propagation during summer and winter over the South China Sea and western North Pacific. *Clim Dyn*. doi:10.1007/s00382-016-3138-z
- Chen TC, Chen JM (1995) An observational study of the South China Sea monsoon during the 1979 summer: onset and life cycle. *Mon Weather Rev* 123:2295–2318
- Chen JP, Wen ZP, Wu R, Chen ZS, Zhao P (2015) Influences of northward propagating 25–90-day and quasi-biweekly oscillations on eastern China summer rainfall. *Clim Dyn* 45(102):105–124
- Chen X, Ling J, Li C (2016) Evolution of Madden–Julian Oscillation in two types of El Niño. *J Clim* 29(5):1919–1934
- Chou S-H, Nelkin E, Ardizzone J, Altas RM (2004) A comparison of latent heat fluxes over global oceans for four flux products. *J Clim* 17:3973–3989
- de Boyer Montégut C, Madec G, Fischer AS, Lazar A, Iudicone A (2004) Mixed layer depth over the global ocean: an examination of profile data and a profile-based climatology. *J Geophys Res* 109:C12003. doi:10.1029/2004JC002378
- Feng X, Wu R, Chen J, Wen ZP (2013) Factors for interannual variations of September–October rainfall in Hainan, China. *J Clim* 26:8962–8978
- Feng J, Liu P, Chen W, Wang XC (2015) Contrasting Madden–Julian Oscillation activity during various stages of EP and CP El Niños. *Atmos Sci Lett* 16:32–37
- Fukutomi Y, Yasunari T (1999) 10–25-day intraseasonal variations of convection and circulation over East Asia and western North Pacific during early summer. *J Meteorol Soc Jpn* 77:753–769
- Gill AE (1980) Some simple solutions for heat-induced tropical circulation. *Q J R Meteorol Soc* 106(449):447–462
- Griffies SM, Harrison MJ, Pacanowski RC, Rosati A (2004) A technical guide to MOM4. GFDL ocean group technical report no. 5. NOAA/Geophysical Fluid Dynamics Laboratory, Princeton, p 342
- Gushchina D, Dewitte B (2012) Intraseasonal tropical atmospheric variability associated with the two flavors of El Niño. *Mon Weather Rev* 140:3669–3681
- Hendon HH, Wheeler M, Zhang C (2007) Seasonal dependence of the MJO-ENSO relationship. *J Clim* 20:531–543
- Huang P, Chou C, Huang R (2011) Seasonal modulation of tropical intraseasonal oscillations on tropical cyclone genesis in the western North Pacific. *J Clim* 24:6339–6352
- Kajikawa Y, Yasunari T (2005) Interannual variability of the 10–25- and 30–60-day variation over the South China Sea during boreal summer. *Geophys Res Lett* 32:L04710. doi:10.1029/2004GL021836
- Kanamitsu M, Ebisuzaki W, Woollen J, Yang SK, Hnilo JJ, Fiorino M, Potter GL (2002) NCEP–DOE AMIP-II reanalysis (R-2). *Bull Am Meteorol Soc* 83:1631–1643
- Kikuchi K, Wang B (2009) Global perspective of the quasi-biweekly oscillation. *J Clim* 22:1340–1359
- Kulkarni A, Kripalani R, Sabade S, Rajeevan M (2011) Role of intraseasonal oscillations in modulating Indian summer monsoon rainfall. *Clim Dyn* 36:1005–1021
- Lindzen RS, Nigam S (1987) On the role of sea surface temperature gradients in forcing low-level winds and convergence in the tropics. *J Atmos Sci* 44:2418–2436
- Liu F, Zhou L, Ling J, Fu X, Huang G (2016a) Relationship between SST anomalies and the intensity of intraseasonal variability. *Theor Appl Climatol*. doi:10.1007/s00704-015-1458-2
- Liu F, Li T, Wang H, Deng L, and Zhang YW (2016b) Modulation of boreal summer intraseasonal oscillations over the western North Pacific by ENSO. *J Clim* accepted
- Mao J, Chan JCL (2005) Intraseasonal variability of the South China Sea summer monsoon. *J Clim* 18(13):2388–2402
- Reynolds RW, Rayner NA, Smith TM, Stokes DC, Wang W (2002) An improved in situ and satellite SST analysis for climate. *J Clim* 15:1609–1625
- Tam CY, Lau NC (2005) Modulation of the Madden–Julian Oscillation by ENSO: inferences from observations and GCM simulations. *J Meteorol Soc Jpn* 83(5):727–743
- Tang Y, Yu B (2008) MJO and its relationship to ENSO. *J Geophys Res* 113:D14106. doi:10.1029/2007JD009230
- Teng H, Wang B (2003) Interannual variations of the boreal summer intraseasonal oscillation in the Asian-Pacific Region. *J Clim* 16:3572–3584
- Wu R (2010) Subseasonal variability during the South China Sea summer monsoon onset. *Clim Dyn* 34:629–642
- Wu R, Cao X (2016) Relationship of boreal summer 10–20-day and 30–60-day intraseasonal oscillation intensity over the tropical western North Pacific to tropical Indo-Pacific SST. *Clim Dyn*. doi:10.1007/s00382-016-3282-5
- Wu R, Kirtman BP (2007) Regimes of local air-sea interactions and implications for performance of forced simulations. *Clim Dyn* 29:393–410
- Wu R, Wang B (2000) Interannual variability of summer monsoon onset over the western North Pacific and the underlying processes. *J Clim* 13:2483–2501
- Wu R, Wang B (2001) Multi-stage onset of the summer monsoon over the western North Pacific. *Clim Dyn* 17:277–289
- Wu R, Hu ZZ, Kirtman BP (2003) Evolution of ENSO-related rainfall anomalies in East Asia. *J Clim* 16:3741–3757
- Wu R, Kirtman BP, Pegion K (2006) Local air-sea relationship in observations and model simulations. *J Clim* 19(19):4914–4932
- Wu R, Cao X, Chen SF (2015) Co-variations of SST and surface heat flux on 10–20-day and 30–60-day time scales over the South China Sea and western North Pacific. *J Geophys Res* 120(24):12486–12499
- Yang J, Wang B, Wang B (2008) Anticorrelated intensity change of the quasi-biweekly and 30–50-day oscillations over the South China Sea. *Geophys Res Lett* 35:L16702. doi:10.1029/2008GL034449
- Ye KH, Wu R (2015) Contrast of local air-sea relationship between 10–20-day and 30–60-day intraseasonal oscillations during May–September over the South China Sea and the western North Pacific. *Clim Dyn* 45(11–12):3441–3459
- Zhang C (2005) Madden–Julian Oscillation. *Rev Geophys*. doi:10.1029/2004RG000158
- Zhang C (2013) Madden–Julian Oscillation: bridging weather and climate. *J Clim* 26:1849–1870
- Zhang C, Gottschalck J (2002) SST anomalies of ENSO and the Madden–Julian Oscillation in the equatorial Pacific. *J Clim* 15:2429–2445
- Zhang LN, Wang BZ, Zeng CQ (2009) Impacts of the Madden–Julian Oscillation on summer rainfall in southeast China. *J Clim* 22:201–216